Characterization of iron-doped lithium niobate for holographic storage applications*

Rajiv R. Shah, Dae M. Kim, T. A. Rabson, and F. K. Tittel

Department of Electrical Engineering, Rice University, Houston, Texas 77001
(Received 4 June 1976; in final form 20 August 1976)

A detailed study of eight systematically chosen Fe:$LiNbO_3$ crystals is presented. Correlation between the photorefractive sensitivity and various chemical properties of Fe:$LiNbO_3$ is investigated in order to ascertain optimum performance of the crystals in holographic storage and display applications. Concentrations of Fe^{2+} and Fe^{3+} ions have been determined from optical and EPR spectra, while impurities have been detected from x-ray-emission and infrared spectra. Particular emphasis is placed on investigating the dependence on Fe^{2+} and Fe^{3+} ion concentrations of the photorefractive sensitivity. The photorefractive sensitivity is shown to depend primarily on the concentration of Fe^{2+} ions in Fe: $LiNbO_3$. This fact seems to suggest that Fe^{2+} ions are the impurity centers responsible for the photorefractive effect in Fe:$LiNbO_3$. Spectral dependence of the photorefractive sensitivity and its modification due to oxygen annealing are also reported. Our results indicate that an unannealed Fe:$LiNbO_3$ crystal containing 0.05 mol% Fe with 20–25% of the ions in the Fe^{2+} state and the remainder in the Fe^{3+} state possesses the most favorable photorefractive sensitivity.

PACS numbers: 42.30.Nt, 42.40.Kw, 42.70.Gi

I. INTRODUCTION

In recent years considerable interest has evolved in certain electro-optic crystals as potential real-time optical storage media capable of efficient, reversible, high-density, and fast recording and display of images or holographic information.[1] The physical mechanism responsible for the formation of phase holograms in such crystals is the photorefractive effect. This process consists of the optical excitation and subsequent transport and retrapping of electrons which originate from localized centers in such crystals.[2,3] Early theories described the transport of charge carriers in terms of diffusion or drift in a constant electric field.[2,3] More recently, Glass *et al.*[4] have suggested a new approach, namely, the charge carriers are photogenerated and displaced in a spatially preferred direction. Photoexcited space-charge patterns resembling the intensity profile of the generating holographic intensity pattern in turn set up electric fields that distort the index of refraction of the crystal through the electro-optic effect. In this manner the refractive-index modulation, which generates a volume phase hologram, can be used as a mechanism for information storage. Although this effect has been observed in several ferroelectric crystals, including $LiNbO_3$,[2,3,5] $LiTaO_3$,[2,5,6] $BaTiO_3$,[7] and SBN,[8] their relatively low recording and erasure sensitivities compared to other direct optical recording media[9] has been a practical drawback. At this time, the most promising of these crystals is $LiNbO_3$, which has a large electro-optic coefficient and whose sensitivity can be increased several orders of magnitude by optimizing the charge transport mechanism. Free electrons are provided by Fe ions present in significant concentrations even in undoped $LiNbO_3$, and substantial improvements in sensitivity have been made by doping $LiNbO_3$ with transition metals, in particular with Fe. Apart from the dependence on total iron concentration, the photorefractive sensitivity of Fe : $LiNbO_3$ is believed to depend also on the concentrations of two valence states of Fe, viz., Fe^{2+} and Fe^{3+}.[10–14] The relative concentrations of Fe^{2+} and Fe^{3+} ions in a given crystal of Fe : $LiNbO_3$ can be altered by subjecting the crystal to oxidizing or reducing heat treatments.[10,11,13] To a lesser extent, the sensitivity can also be improved by applying a large electric field or by writing with short optical pulses.[15]

In view of the importance of improving the photorefractive sensitivity of Fe : $LiNbO_3$ for potential use in holographic storage applications, we report in this paper a detailed characterization of chemical and holographic properties of Fe : $LiNbO_3$. In order to determine optimum crystal properties, we have chosen crystals with a systematic variation of concentrations and crystal treatments. The nature and abundance of impurities present in $LiNbO_3$ affect the photorefractive sensitivity. Impurities have therefore been identified and their concentrations determined by various measurements. These measurements include proton-beam-induced x-ray-emission spectra, ir absorption spectra, optical absorption spectra, and EPR. The absolute concentrations of Fe^{2+} and Fe^{3+} ions for both annealed and unannealed crystals with the same Fe dopant concentrations have been deduced using optical and EPR spectra. Changes in the Fe^{2+} and Fe^{3+} concentrations produced by oxygen annealing are examined. Correlation of the photorefractive sensitivity with concentrations of Fe, Fe^{2+}, and Fe^{3+} has been quantitatively investigated, and the effects of inadvertent impurities in Fe : $LiNbO_3$ are discussed qualitatively. Spectral dependence of photorefractive sensitivity and its modification due to oxygen annealing, and hence also due to reduction, have been studied.

Changes in optical absorption spectra have been ascribed to changes in Fe^{2+} concentrations,[13,14,16] which in turn have been associated with changes in photorefractive sensitivity.[17–19] Fe^{3+} ions in Fe : $LiNbO_3$ have been identified by both EPR spectra[20–22] and magnetic susceptibility measurements.[16] Recently, a direct confirmation of the existence of Fe^{2+} state in $LiNbO_3$ has been made by investigating the Mössbauer spectra of Fe : $LiNbO_3$.[23] In this paper we present comprehensive correlation of these chemical properties with the photorefractive sensitivity of Fe : $LiNbO_3$. Our experimental results and analysis support the suggestion[10,11] that the Fe ion responsible for the increase of absorption in the optical spectrum of Fe : $LiNbO_3$, viz., Fe^{2+}, is also

TABLE I. Relative-concentrations of nickel as determined by proton-beam-induced x-ray emission spectroscopy.

Fe: $LiNbO_3$ crystal	Fe conc. (mol%)	Treatment	(Ni/Nb) (ppm by wt)	$\frac{Ni}{Fe+Ni}$ (%)
x-1	0.005	A	223	47
x-2	0.005	UA	81	29
x-3	0.02	A	108	25
x-4	0.02	UA	83	17
x-5	0.1	A	709	28
x-6	0.1	UA	704	28

mainly responsible for increasing the photorefractive sensitivity. The photorefractive sensitivity increases almost linearly with increasing Fe^{2+} concentration but then saturates; this seems to suggest that in addition to the absolute Fe^{2+} concentration the relative concentrations of Fe^{2+} and Fe^{3+} ions are also important in determining the photorefractive sensitivity. This interpretation is substantiated by the fact that the decrease in photorefractive sensitivity upon oxygen annealing follows a pattern very similar to that of the decrease in Fe^{2+} concentrations (or increase in Fe^{3+} concentrations). As a result, there exist optimum values of Fe, Fe^{2+}, and Fe^{3+} concentrations for which the sensitivity is most favorable—0.05 mol% Fe-doped $LiNbO_3$ with 20—25% Fe^{2+} (and 75—80% Fe^{3+}). It should be noted that in general any further increase in the net cw photorefractive sensitivity of Fe : $LiNbO_3$ will be limited by the accompanying increase in optical absorption without a corresponding increase in the sensitivity.

Furthermore, the diffraction efficiency curves for different crystals are in good agreement with an analytical expression for diffraction efficiency based upon a nonlinear dynamic theory for photorefractive phase hologram formation proposed by the authors.[24,25] This analysis has been used to determine the bulk photovoltaic field as a function of Fe^{2+} concentration and to discuss theoretically the experimentally measured photorefractive sensitivity for various crystals. In Sec. II we present spectroscopic measurements of the physical properties of $LiNbO_3$. In Sec. III are reported the measurements of the photorefractive properties. The analyses and conclusions are presented in Secs. IV and V, respectively.

II. SPECTROSCOPIC MEASUREMENTS OF PHYSICAL PROPERTIES

In order to investigate the dependence of photorefractive sensitivity on iron concentration and on the valence states of iron, Fe : $LiNbO_3$ crystals were chosen with wide-ranging and systematically varying Fe concentrations. Eight crystals were studied, two each with the following Fe dopant concentrations: 0.005, 0.02, 0.05, and 0.1%/mol. A wide range of Fe^{2+} and Fe^{3+} concentrations was obtained by selecting these eight crystals such that four of them were annealed in an oxygen atmosphere while the other four (one of each iron concentration) were not subjected to any heat treatment. The annealing process was done in 1 atm of oxygen for about 24 h at 800—900 °C with a rate of cooling of 100 °C/h. The physical dimensions of the cut and polished crystals[26] were chosen for convenience to be 1 cm (*a* axis) by 0.1 cm (*b* axis) by 1 cm (*c* axis). The following measurements were made on the $LiNbO_3$ crystals.

A. X-ray emission spectra

The presence of impurities in Fe : $LiNbO_3$ other than the main dopant, Fe, can affect the photorefractive sensitivity of Fe : $LiNbO_3$ either adversely or favorably. Therefore, to make any meaningful correlation of the photorefractive sensitivity with the iron concentration, one needs to detect the presence of other impurities and measure their concentrations. The elemental analysis of the crystals was done using two techniques. The first of these techniques employs proton-beam-induced x-ray emission spectroscopy[27] to detect and determine the concentrations of all elements with $Z > 20$ present in the $LiNbO_3$ crystals. Samples analyzed by this technique include the 0.005, 0.02, and 0.1%/mol Fe-doped annealed and unannealed $LiNbO_3$ crystals. Powdered crystals in the form of a thin layer were used as targets for the proton beam.

The measured spectra for all samples show peaks corresponding to Fe and Nb as expected, but they also reveal the unexpected presence of Ni in substantial quantities. In Table I we list the measured concentrations of Ni. Comparison of the concentrations for the annealed and unannealed samples shows that Ni is not introduced by the annealing process, but must enter during growth in the melt or poling. Substantial quantities of Ni in otherwise Fe-doped $LiNbO_3$ crystal can modify the holographic properties of the crystals.[28]

B. ir spectra

Since x-ray emission analysis is limited to elements with $Z > 20$, ir absorption spectroscopy is used to identify impurities with $Z < 20$. In particular hydrogen is an impurity that has been known to enter $LiNbO_3$ crystals and to reduce its photorefractive sensitivity.[29–32] Mechanisms by which hydrogen reduces the susceptibility of $LiNbO_3$ to refractive-index change are not known; but for a proper evaluation of crystal sensitivities and comparison of their performance, one must include the relative concentrations of hydrogen in these crystals. Hydrogen diffuses into the crystals during the poling process and combines with the oxygen in $LiNbO_3$ to form OH ions. The presence of hydrogen in $LiNbO_3$ is manifested by an OH^-, 0—1 stretching vibrational band in the near infrared at approximately 2.86 μm. All eight Fe : $LiNbO_3$ crystals investigated exhibit this band and one of the crystals, the 0.05% Fe-doped annealed crystal, more so than the others (approximately twice—see Fig. 1). The data presented here was taken with a Beckman Type 8 ir spectrophotometer at room temperature. The spectra are unpolarized; however, the *c* axis of the crystal in each case was oriented parallel to the slits and the direction of the beam was perpendicular to the *c* axis. The peak absorptions and hence the relative concentrations of the OH^- ions are shown in Table II. A peak absorption of about 1—2.5 cm^{-1} corresponds to an H-ion concentration of the order of 10^{16}—$10^{17}/cm^3$.[30] The effect of the substantially higher absorption in one of the crystals as compared to the others is discussed in connection with Fig. 11.

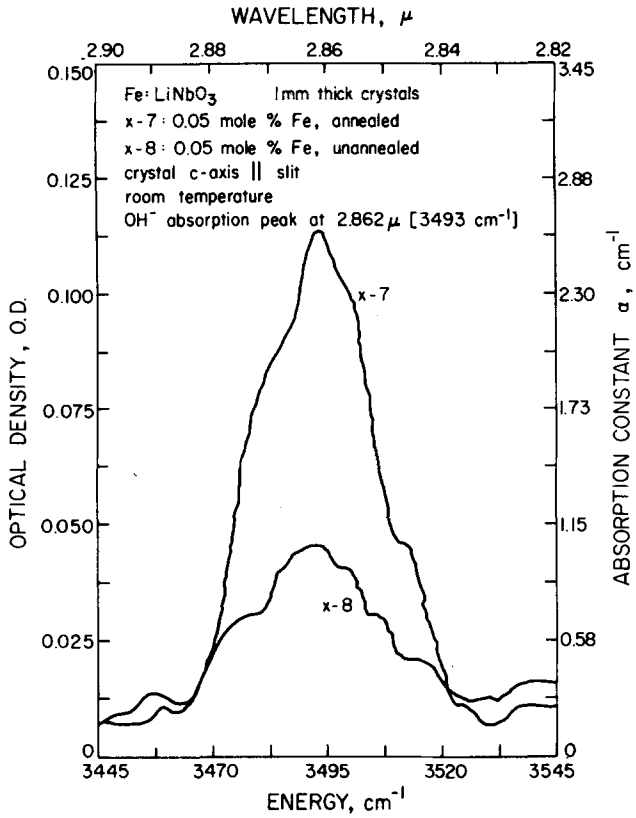

FIG. 1. OH^-, 0—1 stretching vibrational band in the near-infrared absorption spectrum. Spectra for other Fe: $LiNbO_3$ crystals are similar to that of x-8.

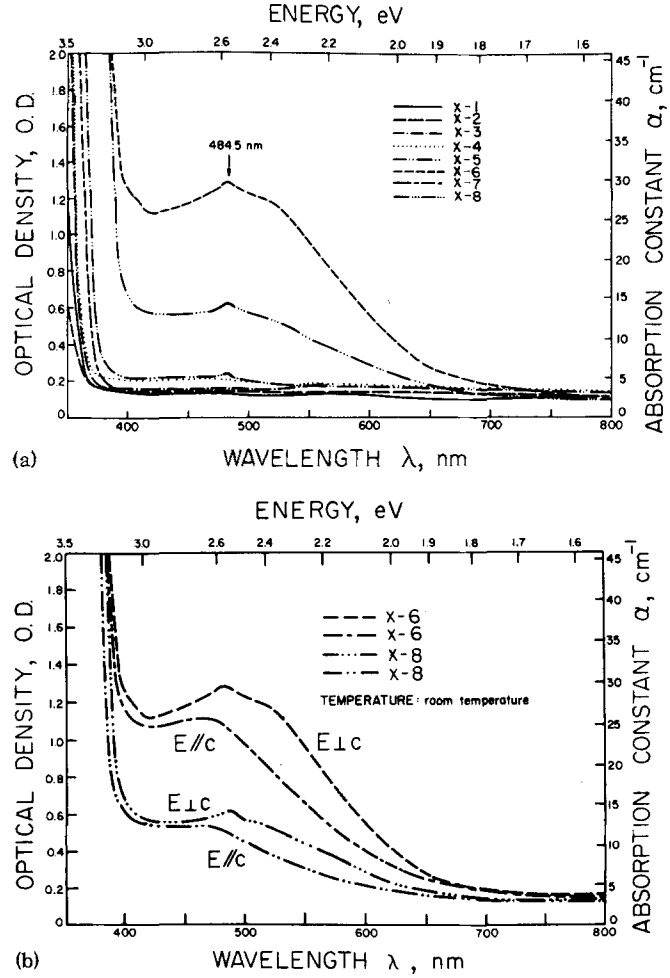

FIG. 2. (a) Optical absorption spectra of all eight Fe: $LiNbO_3$ crystals; polarization $E_\perp c$, (b) polarization dependence of the optical absorption spectrum for 0.05 and 0.1 mol% Fe-doped unannealed $LiNbO_3$ crystals.

C. Optical spectra

Absorption of Fe: $LiNbO_3$ in the visible region of the spectrum is mainly due to the Fe^{2+} state of the iron dopant. The band at 484.5 nm has been attributed to $Fe^{2+} \rightarrow Nb^{5+}$ intervalence charge transfer,[16] and its intensity is proportional to the Fe^{2+} concentration. We have therefore used this band together with the EPR spectra of Fe: $LiNbO_3$ to determine the absolute concentrations of Fe^{2+} and Fe^{3+} ions.

Optical absorption spectra were recorded with a Cary 17 spectrophotometer at room temperature. Spectra for all eight crystals, taken with the beam perpendicular to the c axis for $E \perp c$ (σ spectrum) and $E \| c$ (π spectrum) for each of these crystals are shown in Figs. 2(a) and 2(b). In Fig. 3 the absorption spectral data is replotted to show the change upon oxygen annealing in the intensity of the band at 484.5 nm, and also in the absorption at longer wavelengths in the visible. The intensity of

TABLE II. Relative concentrations of OH^- ions in Fe: $LiNbO_3$ as obtained from near-infrared spectroscopic measurements.

Fe: $LiNbO_3$ crystal	Fe conc. (mol%)	Treatment	OH^- ratios
x-1	0.005	A	1.4
x-2	0.005	UA	1.5
x-3	0.02	A	1.4
x-4	0.02	UA	1.2
x-5	0.1	A	1.0
x-6	0.1	UA	1.0
x-7	0.05	A	3.2
x-8	0.05	UA	1.3

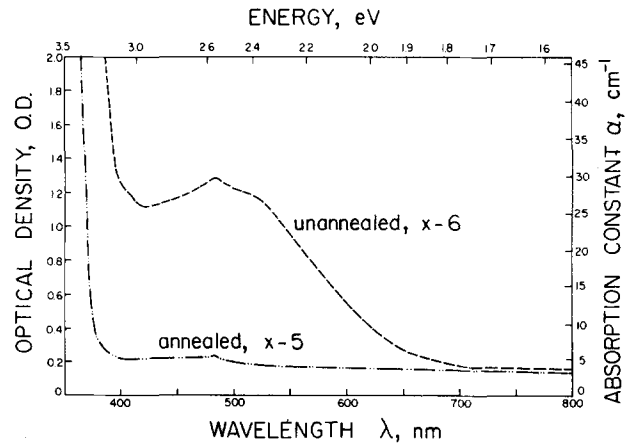

FIG. 3. Effect of oxygen annealing on the optical absorption spectrum for a 0.1 mol% Fe-doped $LiNbO_3$ crystal.

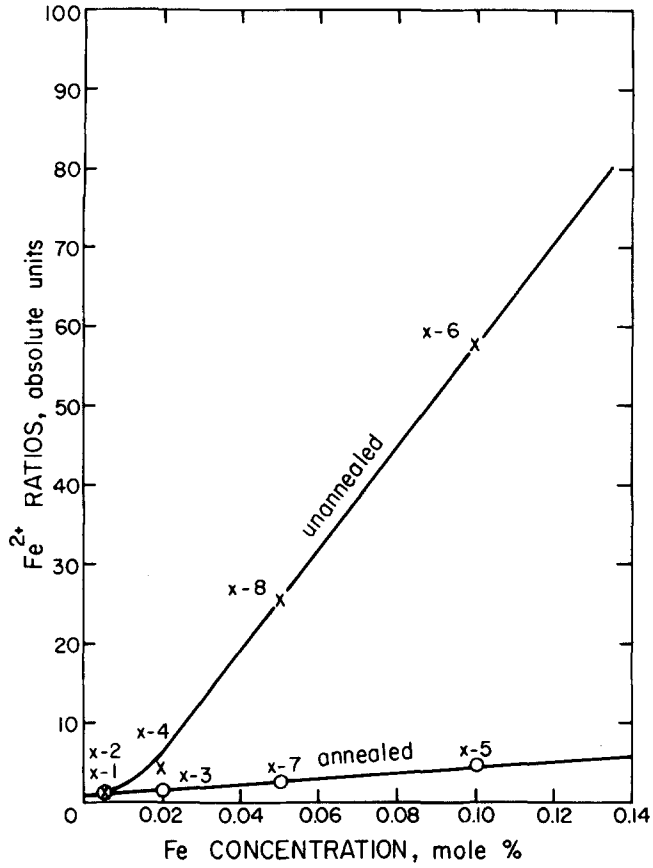

FIG. 4. Relative concentrations of Fe^{2+} in Fe: $LiNbO_3$ calculated from optical absorption data.

the band at 484.5 nm is linear with the Fe concentration for both the annealed and unannealed crystals. Hence the ratios of intensities of this band yield the relative concentrations of Fe^{2+} ions present in each crystal (Fig. 4).

From Figs. 2(a) and 2(b) a marked shift of the absorption edge towards shorter wavelengths upon oxygen annealing is evident. Pure $LiNbO_3$ has an oxygen 2 $p\pi$ valence band and Nb $d\epsilon$ conduction band with a band gap of 3.72 eV.[16] The absorption edge of pure $LiNbO_3$ is therefore at approximately 350 nm. The shift in the absorption edge of $LiNbO_3$ towards longer wavelengths upon doping with Fe is due to the excitation of electrons from the oxygen valence band to the shallow Fe impurity states in the band gap.[16] This shift towards longer wavelengths is greater with increasing Fe concentration, for σ polarization as compared to the π polarization, and for unannealed crystals as compared to annealed crystals, suggesting a modification of the band structure of $LiNbO_3$ by the Fe^{2+} impurities.

D. EPR measurements

Fe^{3+} ions are responsible for the EPR spectrum of Fe : $LiNbO_3$. EPR spectra can therefore be used to calculate the relative concentrations of Fe^{3+} ions in a Fe : $LiNbO_3$ crystal. Hence, with the assumption that all the iron exists either in the divalent or trivalent state it is possible to obtain for any pair of annealed and unannealed crystals with the *same* iron concentration the ratio of their Fe^{2+} and Fe^{3+} contents, obtained independently from optical absorption and EPR data, respectively. In this manner, it is possible to determine the absolute concentrations of Fe^{2+} and Fe^{3+} ions for each of the eight Fe : $LiNbO_3$ crystals under investigation.

For the trigonal C^6_{3v} structure of $LiNbO_3$ and for the Fe substituting for Nb or Li with octahedral coordination with O, the crystal field is approximately axially symmetric. With the inclusion of Zeeman and second-order interactions only, the spin Hamiltonian for Fe^{3+} in $LiNbO_3$ [11,16,20–22] is given by

$$H = g\beta\vec{H}\cdot\vec{S} + D[S_z^2 - \tfrac{1}{3}S(S+1)].$$

The EPR spectrum of single-crystal Fe^{3+} : $LiNbO_3$ exhibits a large orientational dependence and hence is not useful for a comparative study. The EPR analysis was therefore carried out using powdered samples of annealed and unannealed crystals with 0.005, 0.02, and 0.1 mol% Fe.

EPR spectra for each of the six Fe : $LiNbO_3$ crystals mentioned above were taken on a Varian E-line EPR spectrometer at a frequency of 9.3 GHz at 70 °K from 0 to 4000 G (Fig. 5). The absorption peak at approximately 300 G was sufficiently strong to allow a room-temperature measurement in all six samples. This absorption peak corresponds to the transition $|-\frac{1}{2}\rangle \leftrightarrow |-\frac{3}{2}\rangle$ that does not exhibit any angular dependence as described in Ref. 22. A scan was made for each powdered sample over the absorption signal at 300 G. The variation of signal height with change of orientation of the powdered samples with respect to the magnetic field was found to be negligible. However, for each sample an average value of the EPR signal at 300 G was obtained from measurements for four different orientations. The relative magnitudes of the average signal heights for the various samples normalized with respect to sample weight and receiver gain give the relative concentrations of the Fe^{3+} ion in the six Fe : $LiNbO_3$ crystals investigated. Samples of annealed and unannealed 0.05 mol% Fe were not available. However, the concentrations of Fe^{3+} in these two crystals can be estimated from the extrapolation of the graphic representation of this data. The results of the EPR analyses are shown in Fig. 6. We have used these results together

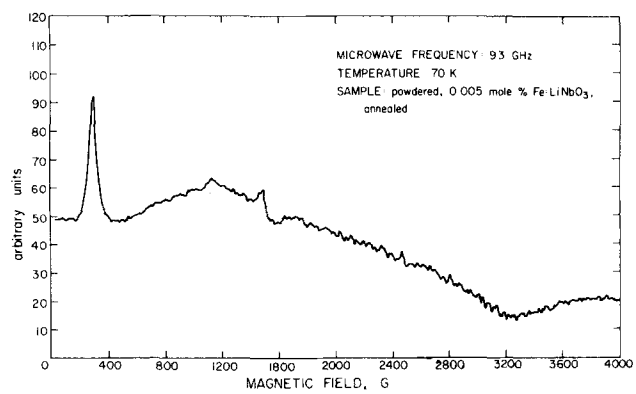

FIG. 5. EPR spectrum of powdered Fe: $LiNbO_3$ (0.005 mol% Fe, annealed).

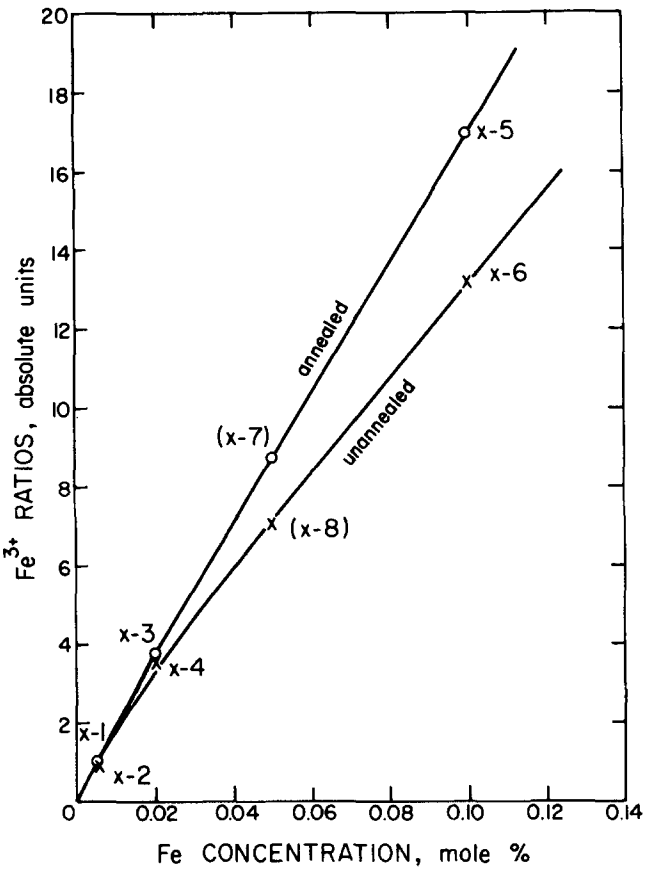

FIG. 6. Relative concentrations of Fe^{3+} ions in Fe: $LiNbO_3$ calculated from EPR measurements.

with those obtained by optical absorption measurement to obtain for any pair of annealed and unannealed Fe : $LiNbO_3$ crystals with a given Fe concentration, the absolute concentrations of Fe^{2+} and Fe^{3+} ions. These results are listed in Table III.

III. MEASUREMENT OF PHOTOREFRACTIVE PROPERTIES

For holographic storage applications the quantity of prime interest is the photorefractive sensitivity. The dependence of photorefractive sensitivity on the physical properties of the crystals and the experimental parameters such as writing and reading wavelengths are important to attain the most favorable storage characteristics and to shed some light upon the physical mechanisms responsible for the process. In this section we

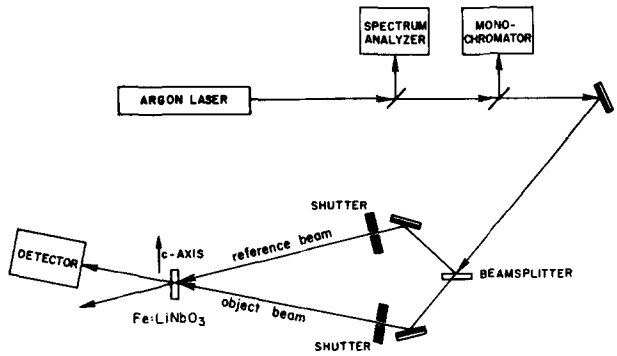

FIG. 7. Experimental arrangement used for measuring photorefractive sensitivity.

discuss the correlation of the diffraction efficiency and photorefractive sensitivity of Fe : $LiNbO_3$ crystals with the experimental data described in Sec. II, such as iron dopant concentration, crystal treatment, and recording wavelength.

A. Experimental arrangement and techniques

Plane-wave holograms were recorded in Fe : $LiNbO_3$ crystals using the experimental arrangement shown in Fig. 7. The coherent radiation source used was an argon ion laser operating in the TEM_{00} transverse mode and a single longitudinal mode with a linewidth of about 50 MHz and a frequency jitter of ± 100 MHz, as monitored by an optical spectrum analyzer. Intensity fluctuations were less than 2% . The optical recording beam was split into a reference beam and an object beam and their intensities were equalized to within 2% using neutral density filters. The two beams, each with a 3-mm diameter, intersected in the crystal at an angle of 12° to form interference fringes in the direction perpendicular to the writing plane. The *c* axis of the crystal was oriented to lie in the writing plane and perpendicular to the bisector of the writing angle. The thickness of the crystals perpendicular to the *c* axis is 1 mm. The incident, reflected, transmitted, and diffracted beams were measured using an EG&G model 580 radiometer.

Holograms were read at the same wavelengths as those used for recording them. This was accomplished by briefly interrupting the recording process at regular intervals of time, blocking one of the recording beams and measuring the diffracted beam without disturbing

TABLE III. Concentrations of Fe^{2+} and Fe^{3+} ions in Fe: $LiNbO_3$ crystals as estimated from optical and EPR spectra.

Fe: $LiNbO_3$ crystal	Fe conc. (mol%)	Treatment	Fe^{2+} conc. (mol%)	Fe^{3+} conc. (mol%)	$\frac{Fe^{2+}}{Fe^{3+}}$	$\frac{Fe^{2+}}{Fe}$ (%)	$\frac{Fe^{3+}}{Fe}$ (%)
x-1	0.005	A	0.4×10^{-3}	$\lesssim 5\times10^{-3}$	...	...	...
x-2	0.005	UA	0.4×10^{-3}	$\lesssim 5\times10^{-3}$	...	...	...
x-3	0.02	A	0.3×10^{-3}	19.7×10^{-3}	0.015	2.0	98
x-4	0.02	UA	1.2×10^{-3}	18.8×10^{-3}	0.064	6.0	94
x-5	0.1	A	0.20×10^{-2}	9.80×10^{-2}	0.019	2.0	98
x-6	0.1	UA	2.40×10^{-2}	7.60×10^{-2}	0.320	24	76
x-7	0.05	A	0.10×10^{-2}	4.90×10^{-2}	0.022	2.0	98
x-8	0.05	UA	1.10×10^{-2}	3.90×10^{-2}	0.280	22	78

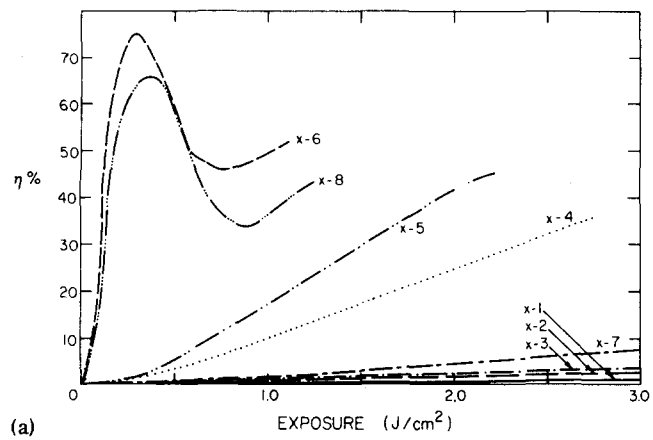

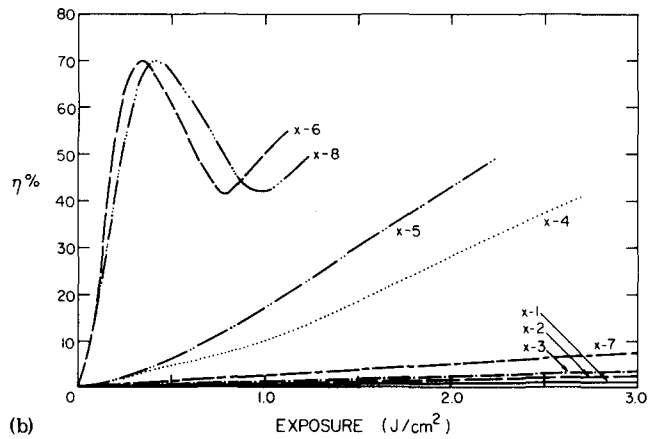

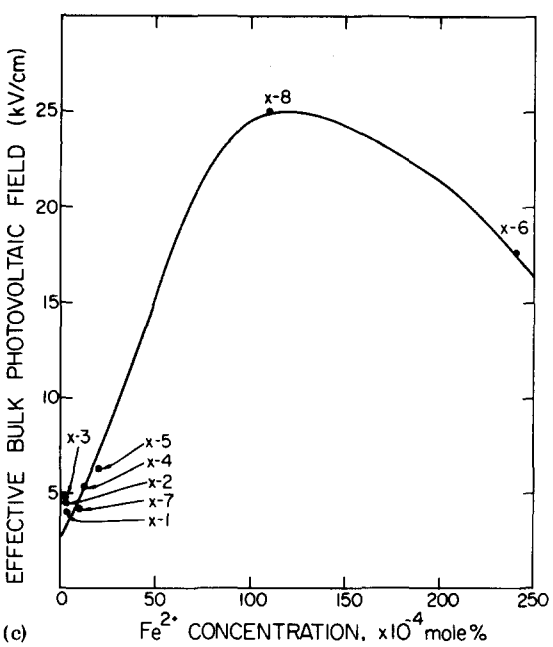

FIG. 8. (a) Dependence of holographic diffraction efficiency curves upon exposure and absorption coefficient for eight Fe: $LiNbO_3$ crystals; (b) theoretically obtained diffraction efficiency curves for the experimental curves of (a). (c) effective bulk photovoltaic field as a function of Fe^{2+} concentration determined from the diffraction efficiency curves.

the system. Six different argon laser lines were used for writing and reading holograms (4574, 4727, 4765, 4880, 4965, and 5145 Å), with the polarization perpendicular to the writing plane. For all crystals and wavelengths, the experimental conditions and the technique for measurement were identical.

B. Definitions of experimental parameters

We now define the quantities in terms of which the experimental results have been measured and interpreted. The diffraction efficiency η of a hologram at a given time t has been defined as the percentage of the initially ($t=0$) transmitted read beam that is diffracted by the hologram at time t. Photorefractive sensitivity is defined as the net energy density required to produce a hologram of a given diffraction efficiency in the initial regime of η. We have incorporated the beam attenuation effect by introducing a parameter

$$\Gamma = [1 - \exp(-\alpha L)]/\alpha L < 1 \qquad (1)$$

(α is the absorption coefficient of the crystal and L is the crystal thickness). The quantity Γ represents the ratio of the average beam intensity inside the crystal to the incident intensity, viz., $I_{avg}/I_0 \equiv \Gamma$. For the ideal case where the crystal has no absorption, $\Gamma = 1$ and $I_{avg} = I_0$. Consequently, this value of I_{avg} will be achieved for a crystal with Γ different from unity if the incident beam I_0 is inversely scaled with respect to Γ, i.e., I_0/Γ. We may thus write the photorefractive sensitivity as

$$S = (\Delta n/\Delta E)\Gamma, \qquad (2)$$

where Δn is the refractive-index change associated with

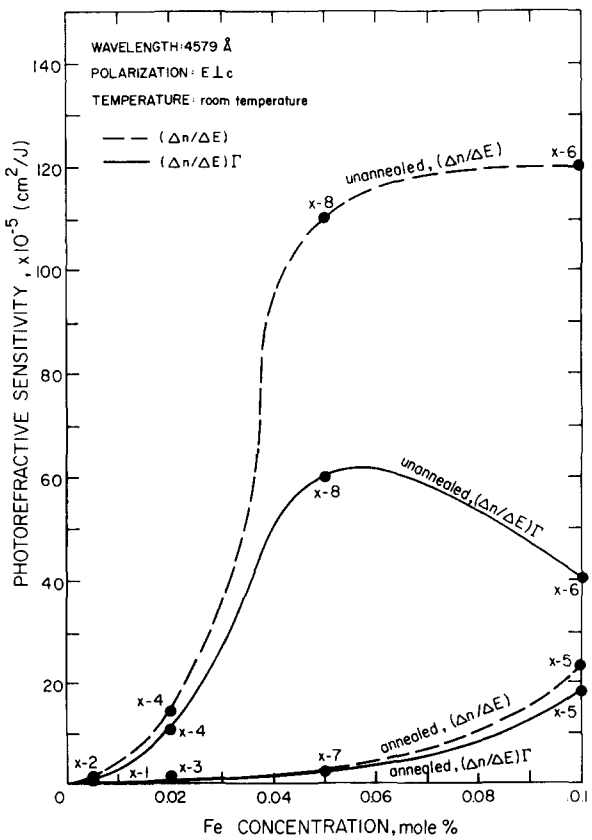

FIG. 9. Dependence of the photorefractive sensitivity on Fe concentration for a set of eight Fe: $LiNbO_3$ crystals, corrected and uncorrected for absorption.

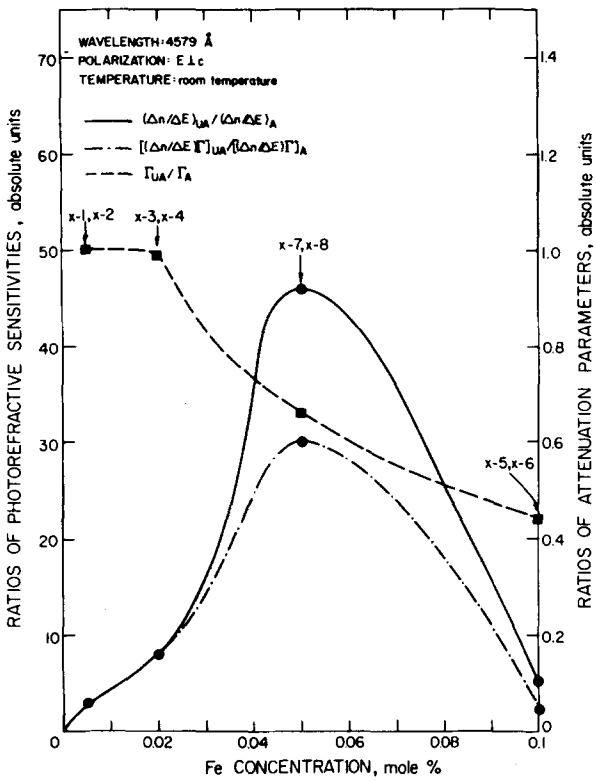

FIG. 10. Comparison of ratios of photorefractive sensitivities and attenuation factors of unannealed and annealed Fe: $LiNbO_3$ crystals of the same Fe concentration.

a fixed value of η (10%) and ΔE is the incident energy density required to produce it.[33]

C. Experimental results

The experimentally measured diffraction efficiency curves for all eight Fe : $LiNbO_3$ crystals are depicted in Fig. 8(a). Due to the differences in intensities used for recording holograms in these crystals, the abscissa has been taken to be the writing energy density or exposure instead of time. We have adopted this procedure in view of the fact that reciprocity between intensity I and writing time t has been observed and reported previously[25] [see Fig. 1(b) in Ref. 25].

Increase in the initial slope of the η curves with increasing Fe concentration is evident from Fig. 8(a). Also it is clear that the slope of the η curves is substantially higher for the unannealed crystals as compared to that of the annealed crystals of the same Fe concentration. Furthermore, for crystals with low Fe concentration, η curves are monotonically increasing in the exposure investigated, whereas within the same exposure range crystals with high Fe concentration show the remarkable oscillatory behavior previously discussed.[25] The effect of Fe^{2+} concentration or α on the time scale in which the space-charge field builds up is already evident in the initial region of the η curves. This will be discussed in greater detail in Sec. IV.

The dependence of photorefractive sensitivity on iron concentration and crystal treatment is shown in Fig. 9. To emphasize the effect of absorption in the crystal, photorefractive sensitivities without the attenuation parameter Γ are also plotted in Fig. 9. Note the great difference in the sensitivities of the unannealed and annealed crystals. For the unannealed crystals a saturation is seen in the photorefractive sensitivity as a function of Fe concentration without the inclusion of attenuation effects. With the inclusion of Γ the photorefractive sensitivity for the unannealed crystals increases with increasing Fe concentration, reaches a maximum value, and then decreases again, thus indicating the predominance of absorption in crystals with high Fe concentration. The effect of absorption in the crystal can thus be judged from the difference in the sensitivity curves with and without the factor Γ. The annealed crystals, which have a much lower sensitivity, show only a slight modification when taking into account the absorption parameter Γ. In Fig. 10 are plotted the ratios of the photorefractive sensitivities (with and without the attenuation parameter Γ) of the unannealed to those of the annealed crystals of the same Fe concentration and the ratios of their corresponding Γ's. First, since the ratios of sensitivities are greater than unity for all crystals, all unannealed crystals have higher sensitivities than their annealed counterparts. This is to be expected from the results of Fig. 9. For crystals with low Fe concentration, attenuation effects are negligible and the curves of the ratios of photorefractive sensitivities with and without the attenuation factor Γ almost coincide. For crystals with high Fe concentration the effective sensitivity is not enhanced because of the counteracting influence—the beam attenuation factor. For example, for the 0.1%/mol Fe-doped crystal $\Gamma_{UA}/\Gamma_A \approx 0.44$ and $(\Delta n/\Delta E)_{UA}(\Delta n/\Delta E)_A^{-1} \approx 5$. On the other hand, for the 0.05%/mol Fe-doped crystal, $\Gamma_{UA}/\Gamma_A \approx 0.66$ and $(\Delta n/\Delta E)_{UA}(\Delta n/\Delta E)_A^{-1} \approx 46$, i.e., the gain in photorefractive sensitivity is far greater than the increase in absorption of the unannealed crystal. This

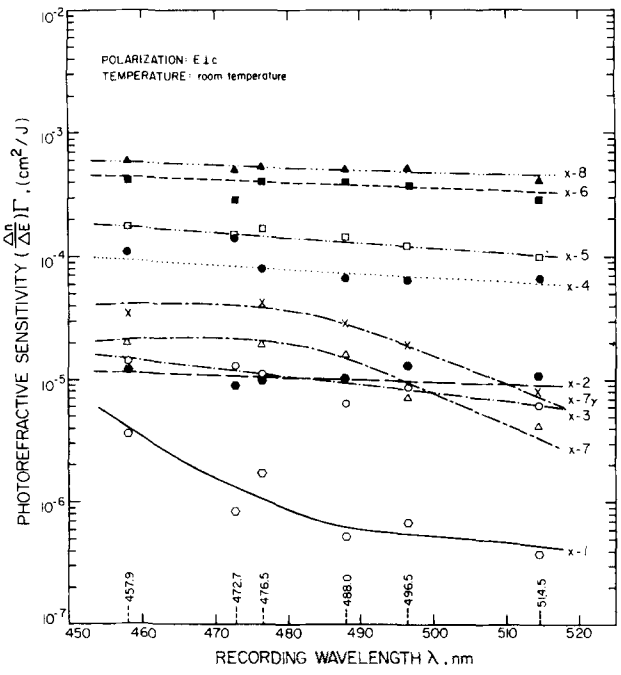

FIG. 11. Spectral dependence of photorefractive sensitivity for a set of eight Fe: $LiNbO_3$ crystals.

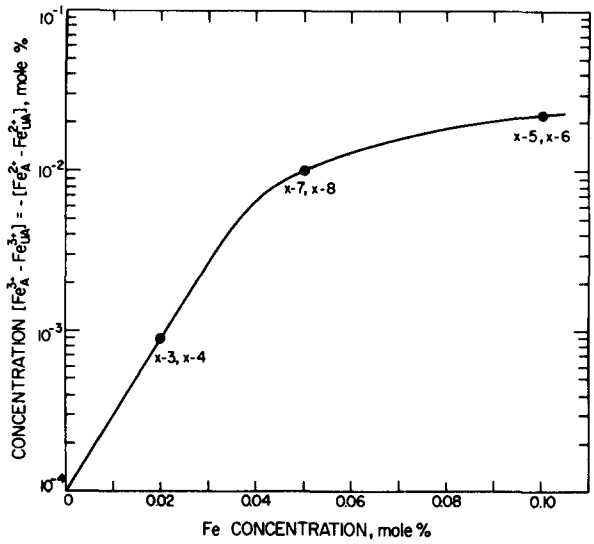

FIG. 12. Effect of oxygen annealing on Fe^{2+} and Fe^{3+} concentrations.

shows explicitly that the optimal region for recording phase holograms in unannealed Fe : $LiNbO_3$ with high photorefractive sensitivity and low absorption is 0.04—0.07%/mol Fe.

The spectral dependence of the photorefractive sensitivity for all eight Fe : $LiNbO_3$ crystals is shown in Fig. 11. Six different wavelengths were used: 4579, 4727, 4765, 4880, 4965, and 5145 Å. It is evident from

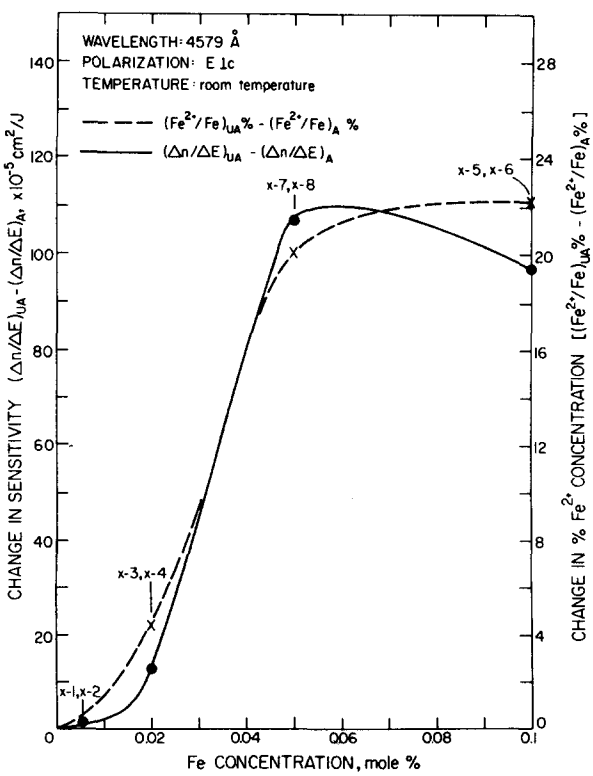

FIG. 13. Comparison of change in photorefractive sensitivity and change in percentage of Fe^{2+} concentrations for a set of eight Fe : $LiNbO_3$ crystals.

Fig. 11 that photorefractive sensitivities of all crystals except x-1 and x-7, within the limits of experimental error, increase linearly with decreasing wavelength. It is interesting to compare the spectral dependence of the photorefractive sensitivity with that of optical absorption (see Figs. 2 and 3); while the optical absorption shows a distinct peak and decreases with decreasing wavelength near 4845 Å, no such dependence is observed in the sensitivity curve.

For two crystals, x-1 and x-7 the spectral dependence of sensitivity departs from the general linear behavior (Fig. 11). From the data given in Tables I and II, it can be seen that crystal x-1 has a high Ni concentration while crystal x-7 has a high OH^- concentration as com-

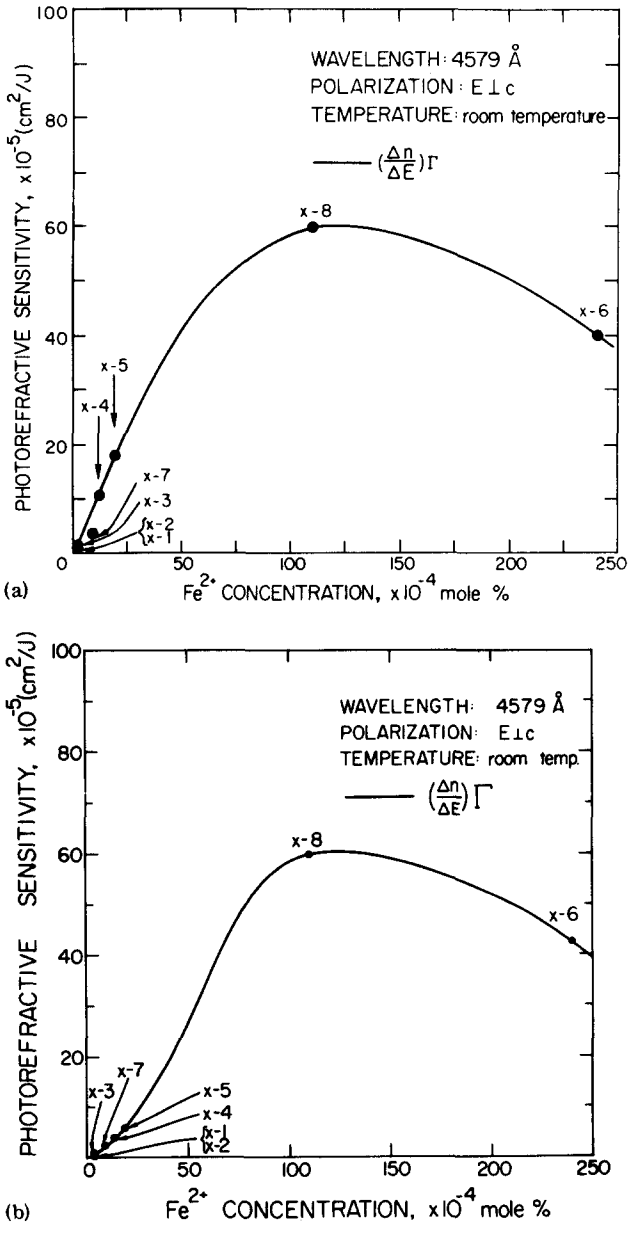

FIG. 14. (a) Dependence of photorefractive sensitivity of a set of eight Fe : $LiNbO_3$ crystals on Fe^{2+} concentrations; (b) theoretically obtained photorefractive sensitivity as a function of Fe^{2+} concentration.

pared to the other crystals. We may qualitatively explain the general shapes of the sensitivity curves for x-1 and x-7 as follows. OH^- ions modify the transport properties of the crystal so as to enhance the sensitivity for short wavelengths and reduce it for long wavelengths.[29–32] For x-1, the higher concentration of Ni, which has a high absorption at shorter wavelengths plotted in Fig. 11 (Ref. 34), increases the sensitivity, while for λ close to 5000 Å Ni does not have a high absorption and hence does not enhance the sensitivity. As a result the shape of the photorefractive sensitivity curve for λ close to 5000 Å does not depart from the general linear behavior exhibited by the other crystals. Crystal x-7 was subjected to γ radiation from a 7-mCi source for about seven days in the course of Mössbauer measurements. This resulted in a slightly increased sensitivity (curve x-7 γ in Fig. 11), possibly due to the creation of defect centers, but there is no change in the general shape of the sensitivity curve.

IV. ANALYSIS

Based on the data given in Secs. II and III, we now consider the role played by the two valence states of iron, i.e., Fe^{2+} and Fe^{3+} in the photorefractive effect. In particular, we examine the effect of oxygen annealing and establish the correlation between photorefractive sensitivity and Fe^{2+} concentration. In addition, with the aid of our theory[24,25] we relate crystal parameters to the diffraction efficiency and the photorefractive sensitivity.

Figure 12 shows the increase in the absolute concentration of Fe^{3+} ions upon oxygen annealing of $Fe:LiNbO_3$. On a logarithmic scale, the Fe^{3+} concentration increases linearly with the Fe concentration in the crystal up to about 0.04%/mol Fe, but then begins to saturate. Another way of stating this saturation is that with increasing Fe concentration the fractional occupancy of the Fe^{3+} state (Fe^{3+}/Fe) in the unannealed crystal decreases (see Table III).

We examine the dependence of photorefractive sensitivity on the concentrations of the two valence states of iron. In Sec. III we have investigated photorefractive sensitivity as a function of Fe concentration separately for the annealed and unannealed crystals (see Fig. 9). We now consider the dependence of photorefractive sensitivity on the Fe^{2+} ion concentrations. The differences in (a) sensitivities of the annealed and unannealed crystals and (b) the corresponding percentages of Fe^{2+} ions are plotted in Fig. 13 as a function of Fe concentration. The remarkable similarity in the two curves shows explicitly a direct relation between photorefractive sensitivity and Fe^{2+}-ion concentration.

We plot in Fig. 14(a) photorefractive sensitivity directly as a function of the absolute Fe^{2+} concentration in these crystals (Table III). Note that unlike Fig. 9, where the photorefractive sensitivities for the annealed and unannealed crystals lie on two separate curves, we have in Fig. 14(a) a single curve for photorefractive sensitivity regardless of whether the crystal is annealed or not annealed, depending only on their Fe^{2+} concentrations. No such dependence is seen on Fe^{3+} concentrations, for which we once again have separate plots for the annealed and unannealed crystals, as in Fig. 9. From Fig. 14(a) it can be seen that the photorefractive sensitivity increases initially as a linear function of the Fe^{2+} concentration, just as in the case of optical absorption (Fig. 4), but then begins to decrease. We will discuss this point further in the following paragraphs.

First we analyze the experimentally obtained diffraction efficiency (η) curves [see Fig. 8(a)]. In Ref. 25 the intensity response of the bulk photovoltaic field E for a single crystal was investigated by means of the η curves. There a systematic relationship between the writing beam intensity and the time scale was observed in good agreement with the nonlinear dynamic theory for the space-charge field.[24] In this work, however, an emphasis is placed on examining the response of η to crystal parameters, in particular to Fe^{2+} concentration. As in the previous case,[25] η curves can be described for a given crystal by the same formulation.[24] The space-charge field or η evolves in time scaled with the crystal parameters and intensity as

$$t/\tau_g = (e\mu\tau/\epsilon)(\alpha I t/\hbar\omega) \tag{3}$$

[see Eqs. (5) and (6) in Ref. 24]. Here e, μ, τ, and ϵ denote the electronic charge, mobility, trapping time and permittivity of the crystal, respectively.

In addition, η depends very sensitively on the effective electron drift field [see Eqs. (2) and (3) in Ref. 25]. Crystals investigated herein have a very wide range of Fe^{2+} concentration. Hence one cannot assume a common photovoltaic field E for the entire set of these crystals, but should regard E as a function of the donor concentration.[4,36] In fact, since η is an explicit function of the coupling strength of the phase grating [Eqs. (2) and (3) in Ref. 25], which in turn depends on the exposure and the effective drift field E, one can determine from the experimental η curves, with the neglect of diffusion, the values of E for the corresponding crystals. In Fig. 8(b) we have plotted the theoretical η curves for the crystals investigated, and these curves are in good agreement with the experimental results [Fig. 8(a)]. In Fig. 8(c) we present the corresponding E values as a function of Fe^{2+} concentration. These E values have been obtained at a common exposure, since E in general can also be a function of intensity.[25] Note an interesting similarity between Fig. 8(c) and the results of Krätzig and Kurz.[36]

As pointed out previously, the values of sensitivity plotted in Fig. 14(a) were obtained in the initial regime of η. In this initial regime[24,25,35] the refractive-index modulation is proportional to the exposure as well as the equivalent electron drift field due to the bulk photovoltaic effect,[4] while η is proportional to the square of the refractive-index modulation. Hence the photorefractive sensitivity in this regime of η reads as

$$S = [\tfrac{1}{2} n_e^3 r_{33} e\mu\tau)/\epsilon\hbar\omega Z]\alpha\Gamma[L^{-1}\int_0^L dz\, \exp(-2\alpha z)E^2(z)]^{1/2}, \tag{4}$$

where the extraordinary index of refraction $n_e = 2.27$, the electro-optic coefficient $r_{33} = 3.08\times10^{-11}$ m/V, e is the electronic charge, the mobility $\mu = 15\times10^{-4}$ m^2/V sec,

TABLE IV. Comparison of the most favorable photorefractive sensitivity with previously published sensitivity data (Ref. 15) for writing with short high intensity pulses. (The high sensitivity in Ref. 15 was attributed to multiphoton photorefractive processes.)

Crystal	Writing technique	$\Delta n/\Delta E$ (cm^2/J)	α (cm^{-1})	Γ	$(\Delta n/\Delta E)\Gamma$ (cm^2/J)
Bell Labs	cw at 5145 Å	3.6×10^{-6}	0.72	0.93	3.4×10^{-6}
0.05% Cu^{2+}: $LiNbO_3$	50 MW/cm^2	4.1×10^{-5}	0.25	0.98	4.0×10^{-5}
	10-ps pulses at 5300 Å				
	500 MW/cm^2				
	10-ps pulses at 5300 Å	3.1×10^{-4}	2.5	0.79	2.4×10^{-4}
Rice Crystal	cw at 5145 Å	7.3×10^{-4}	12.9	0.56	4.1×10^{-4}
0.05% Fe: $LiNbO_3$ unannealed	cw at 4579 Å	11×10^{-4}	13.5	0.55	6.0×10^{-4}
undoped $LiNbO_3$	cw at 5145 Å	$\sim10^{-9}$	$<10^{-2}$	1	$\sim10^{-9}$

the trapping time $\tau = 6\times10^{-11}$ sec, the dielectric constant $\epsilon = 2.83\times10^{-10}$ F/m, wavelength $\lambda = 4579$ Å, the characteristic impedance of free space $Z = 377\ \Omega$, the absorption coefficient $\alpha = 1350\ m^{-1}$, and the attenuation parameter $\Gamma = 0.549$. Thus Eq. 4 gives the sensitivity in terms of crystal parameters, beam attenuation, and the equivalent electron drift field, $E(z)$. We can now discuss Fig. 14(a) theoretically by explicitly evaluating Eq. 4. In so doing we use the values of E obtained in Fig. 8(c). These experimentally determined E values correspond to the field averaged over the crystal depth and hence can be taken out of the integral. The theoretically obtained values for photorefractive sensitivity are plotted in Fig. 14(b) which is in fairly good agreement with the experimental curve of Fig. 14(a).

V. CONCLUSIONS

We have carried out a detailed and methodical study of eight systematically chosen Fe: $LiNbO_3$ crystals. As a result, we have

(1) determined the concentration of Fe^{2+} and Fe^{3+} ions in Fe: $LiNbO_3$ from optical absorption and EPR measurements,

(2) established the relation between the photorefractive sensitivity and Fe^{2+} and Fe^{3+} concentrations,

(3) investigated the spectral dependence, the effect of oxygen annealing, and of other impurities on the photorefractive sensitivity,

(4) analyzed the diffraction efficiency curves for different crystals and corresponding sensitivities with the dynamic theory of hologram formation, and

(5) determined the bulk photovoltaic fields as a function of Fe^{2+} concentrations.

We have shown in the course of this work that for the crystals examined by us there exists an optimal set of crystal characteristics for which the photorefractive sensitivity is most favorable. The optimal parameters are (a) 0.05%/mol Fe concentration, (b) $Fe^{2+}/Fe \sim 20$–25%, (c) $\alpha \sim 13.5\ cm^{-1}$, and (d) crystal thickness 0.1 cm. For these parameters, the sensitivity has been observed to be $6\times10^{-4}\ cm^2/J$ at 4579 Å. We compare this sensitivity with the sensitivities reported in the literature and have summarized it in Table IV.

ACKNOWLEDGMENTS

The authors wish to express their appreciation to Dr. Graham Palmer for helping with the EPR measurements and to Dr. V. Valkovic for taking the x-ray emission spectra.

*Work supported by the National Aeronautics and Space Administration.

[1]Di Chen and J.D. Zook, Proc. IEEE **63**, 1207 (1975).
[2]F.S. Chen, J. Appl. Phys. **40**, 3389 (1969).
[3]J.J. Amodei and D.L. Staebler, RCA Rev. **33**, 71 (1972).
[4]A.M. Glass, D. von der Linde, and T.J. Negran, Appl. Phys. Lett. **25**, 233 (1974).
[5]F.S. Chen, R.T. Denton, K. Nassau, and A.A. Ballman, Proc. IEEE **56**, 782 (1968).
[6]H. Tsuya, J. Appl. Phys. **46**, 4323 (1975).
[7]R.L. Townsend and J.T. LaMacchia, J. Appl. Phys. **41**, 5188 (1970).
[8]J.B. Thaxter, Appl. Phys. Lett. **15**, 210 (1969).
[9]J. Bordonga, S.A. Keneman, and J.J. Amodei, RCA Rev. **33**, 227 (1972).
[10]G.E. Peterson, A.M. Glass, and T.J. Negran, Appl. Phys. Lett. **19**, 130 (1971).
[11]G.E. Peterson, A.M. Glass, A. Carnevale, and P.M. Bridenbaugh, J. Am. Ceram. Soc. **56**, 278 (1973).
[12]P.L. Shah, T.A. Rabson, F.K. Tittel, and T.K. Gaylord, Appl. Phys. Lett. **24**, 130 (1974).
[13]W. Phillips and D.L. Staebler, J. Electron. Mater. **3**, 601 (1974).
[14]D.L. Staebler and W. Phillips, Appl. Opt. **13**, 788 (1974).
[15]D. von der Linde, A.M. Glass, and K.F. Rodgers, Appl. Phys. Lett. **25**, 155 (1974).
[16]M.G. Clark, F.J. Disalvo, A.M. Glass, and G.E. Peterson, J. Chem. Phys. **59**, 6209 (1973).
[17]B. Dischler, J.R. Herrington, A. Räuber, and H. Kurz, Solid State Commun. **14**, 1233 (1974).
[18]B. Dischler and A. Räuber, Solid-State Commun. **17**, 953 (1975).
[19]H. Kurz and E. Krätzig, Appl. Phys. Lett. **26**, 635 (1975).
[20]F. Mehran and B.A. Scott, Solid State Commun. **11**, 15 (1972).
[21]J.R. Herrington, B. Dischler, and J. Schneider, Solid State Commun. **10**, 509 (1972).
[22]H.H. Towner, Y.M. Kim, and H.S. Story, J. Chem. Phys. **56**, 3676 (1972).
[23]W. Keune, S.K. Date, I. Dezsi, and U. Gonser, J. Appl. Phys. **46**, 3914 (1975).
[24]Dae M. Kim, Rajiv R. Shah, T.A. Rabson, and F.K. Tittel, Appl. Phys. Lett. **28**, 338 (1976).

[25]Dae M. Kim, Rajiv R. Shah, T.A. Rabson, and F.K. Tittel, Appl. Phys. Lett. **29**, 84 (1976).
[26]Crystals purchased from Crystal Technology, Inc., Mountain View, Calif.
[27]V. Valkovic, R.B. Liebert, T. Zabel, H.T. Larson, D. Miljanic, R.M. Wheeler, and G.C. Phillips, Nucl. Instrum. Methods **114**, 573 (1974).
[28]D.L. Staebler and W. Phillips, Appl. Phys. Lett. **24**, 268 (1974).
[29]H.J. Levinstein, A.A. Ballman, R.T. Denton, A. Ashkin, and J.M. Dziedzic, J. Appl. Phys. **38**, 3101 (1967).
[30]R.G. Smith, D.B. Fraser, R.T. Denton, and T.C. Rich, J. Appl. Phys. **39**, 4600 (1968).
[31]S. Singh, H.J. Levinstein, and L.G. Van Uitert, Appl. Phys. Lett. **16**, 176 (1970).
[32]J.R. Herrington, B. Dischler, A. Rauber, and J. Schneider, Solid State Commun. **12**, 351 (1973).
[33]For x-1 the photorefractive sensitivity was calculated at an η value of 2%, due to the long time that would be needed to write a hologram in that crystal to 10% diffraction efficiency.
[34]W. Phillips, J.J. Amodei, and D.L. Staebler, RCA Rev. **33**, 94 (1972).
[35]L. Young, W.K.Y. Wong, M.L.W. Thewalt, and W.D. Cornish, Appl. Phys. Lett. **24**, 264 (1974).
[36]E. Krätzig and H. Kurz, 149th Meeting of the Electrochemical Society, Washington, D.C., 1976 (unpublished).